Channel Cross-Coupling in a Polymer-Based Single-Mode Bus Array

Suning Tang, Ray T. Chen, *Member, IEEE,* Rob Mayer, Dave Gerold, Tomasz Jannson, and Andrew Kostrzewski

***Abstract*— In this paper, a crosstalk model is developed to study the packing density and interconnect distance limitations of an optical interconnect system employing polymer-based single-mode bus arrays. The upper limit of channel packing density (1250 channels/cm at interconnect distance of 5 cm) is determined for the first time using the crosstalk model, in which channel cross-coupling among an infinite number of waveguides is considered. Computer simulations are provided together with the proven experimental results. It is shown that there is a threshold of channel separation due to channel cross-coupling, which results in a tradeoff between channel packing density and interconnect distance. Waveguide dimension closer to the cutoff boundary of second mode (E_{12}^x) is preferred for an optimum design.**

OPTICAL bus arrays are attractive for optical interconnect systems because of their low crosstalk, small propagation loss, and parallel operation with high packing density [1]–[4]. Optical bus arrays are used in massively parallel optical interconnects [5], integrated-optic star couplers [6], optical splitters, and waveguide gratings [7], [8]. Important criteria in determining the usefulness of optical bus arrays are their interconnect distance and packing density, which may be limited by the channel cross-coupling, and therefore has been investigated in some detail. The early investigation showed that the crosstalk noise due to channel cross-coupling must be smaller than -12 dB for incoherent light and -32 dB for coherent light using a 1-dB power penalty criterion at a bit-error-rate (BER) of 10^{-15} [9].

In this paper, the limitations on packing density and interconnect distance are investigated for the first time on a polymer-based single-mode bus array (PBSMBA). A crosstalk model is developed based on coupled-model theory [10], [11]. An infinite number of cross-coupled buses is considered, and an exact simulated solution is presented together with the experimental results. It is shown that there is a threshold of acceptable packing density due to bus cross-coupling. For an optimum design, large waveguide dimension up to the cutoff boundary of second mode (E_{12}^x) is preferred. The analysis developed herein is applicable not only to the photolime gel PBSMBA's but also to single-mode optical bus arrays based on other materials.

Manuscript received ; revised August 8, 1994. This work was supported by Cray Research, Inc., Physical Optics Corporation, BMDO and the University of Texas at Austin.

S. Tang, R. T. Chen, R. Meyer, and D. Gerold are with the Microelectronics Research Center, Department of Electrical and Computer Engineering, University of Texas, Austin, TX 78712-1084 USA.

T. Jannson and A. Kostrzewski are with the Physical Optics Corporation, Torrance, CA 90505 USA.

IEEE Log Number 9406484.

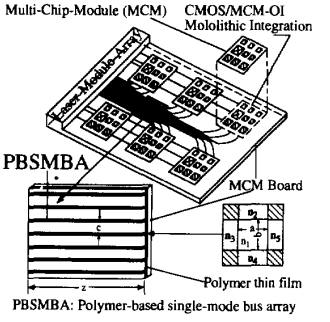

Fig. 1. A schematic diagram of a MCM board using PBSMBA, where the cross-section of a channel waveguide under consideration is also shown.

The following describes the geometry used in our analysis. We consider an optical bus array using identical single-mode channel waveguides with uniform channel separation. The schematic of the device presented is shown in Fig. 1, where a single-mode channel waveguide array based on photolime gel polymer is employed as an optical bus array on a multichip-module (MCM) board [5]. The square single-mode channel waveguide is selected, with the channel width (a) equal to the channel depth (b). Here n_1 and n_{2-5} are the refractive indexes of the guiding layer and cladding layers, respectively. The cross section of a channel waveguide is also depicted in Fig. 1. The lateral index difference ($n_1 - n_{3,5}$) of up to 0.2 can be produced by the photo-induced index modulation, and the vertical index difference ($n_1 - n_4 \sim 0.01$) is due to the graded index effect of our polymer. $n_1 = 1.5$ and $n_2 = 1.0$ are the index of our polymer and index of air, respectively. The dimensions of a single-mode channel waveguide are dependent on all refractive indexes and on the operating wavelength [4], [5].

Based on coupled-mode theory, the complex field in the nth channel obeys the equation [10], [11]

$$\frac{E_n(z)}{dz} = -i\kappa E_{n-1}(z) - i\kappa E_{n+1}(z) - \frac{\alpha}{2}E_n(z) \qquad n = 0, \pm 1, \pm 2, \cdots \tag{1}$$

where n represents the nth channel waveguide, α is a single waveguide absorption coefficient, z is the length of channel waveguide array, and κ is the coupling coefficient between two adjacent waveguides. For a well-confined single-mode channel

waveguide array with $a = b$, we have [12]

$$\kappa = -i\frac{\exp(-c/\xi)}{a\xi(2\pi n_1/\lambda - 2/\xi)} \tag{2}$$

where λ is the operating wavelength, c is the channel separation, and $\xi = \xi_3 = \xi_5$ represents the penetration depth of the field components in cladding media 3 and 5. ξ is given by

$$\xi = \frac{A}{\pi}\left\{1 - \left[\frac{\pi A}{\pi a + 2A}\right]^2\right\}^{-0.5} \tag{3}$$

where $A = \frac{\lambda}{2}(n_1^2 - n_{3,5}^2)^{-0.5}$. Note that ξ is primarily determined by a, n_1, n_3, and n_5 rather than b, n_2, and n_4.

When the input energy for each channel is equivalent, the boundary condition of (1) is $|E_0(0)| = |E_n(0)| = E_0$. The solution to (1) for the center channel, can then be written as

$$E_0(z) = \left\{E_0 J_0(2i\kappa z) + \sum_{n=\infty}^{\infty}[E_n(0)(-i)^n J_n(2i\kappa z)]\right\} \times \exp\left(-\frac{1}{2}\alpha z\right) \qquad n \neq 0 \tag{4}$$

where J_0 and J_n represent the fundamental and nth order Bessel functions. The term $\exp(-\frac{1}{2}\alpha z)$ is due to waveguide propagation loss. The term $J_0(2i\kappa z)$ accounts for the signal remaining in its own channel, whereas higher order Bessel functions account for undesired crosstalk from other channels. Such crosstalk causes either noise increase or signal decrease. Note that the center channel experiences the most cross-coupling.

The crosstalk intensity to the center channel, based on (4), can thus be written as

$$I_{\text{coh}} = \left|\sum_{n=\infty}^{\infty}[E_n(0)(-i)^n J_n(2i\kappa z)]\right|^2 \exp(-\alpha z), n \neq 0, \tag{5}$$

$$I_{\text{inc}} = |2E_0|^2\left\{\sum_{n=1}^{\infty}[J_n(2i\kappa z)]^2\right\}\exp(-\alpha z), \tag{6}$$

for coherent and incoherent light, respectively. With coherent light sources, the phase relationship among all channels should be considered as well. To provide a conservative design criterion, we consider the worst case crosstalk where the cross-coupling noise from all other channels are in phase at the center channel and thus to give rise to the maximum noise level. With this condition, (5) becomes

$$I_{\text{coh}} = |2E_0|^2\left\{\left[\sum_{n=2m}^{\infty} J_n(2i\kappa z)\right]^2 + \left[\sum_{n=2m+1}^{\infty} J_n(2i\kappa z)\right]^2\right\} \times \exp(\alpha z). \quad m = 1, 2, 3\cdots. \tag{7}$$

The effect of waveguide propagation loss will be neglected in this paper because it only changes the power budget required rather than the crosstalk figure (see (6), (7), and (8)). Note that the optical propagation loss was determined as low as 0.1 dB/cm in polymer-based channel waveguide fabricated by optical cross-link technique [5], [13] and as low as 0.5 dB/cm fabricated by compression-molding technique [4].

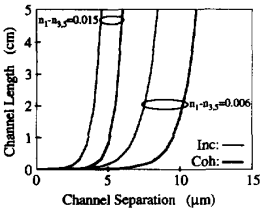

Fig. 2. Channel length versus channel separation to ensure a minimum of 32 dB and 12 dB S/N ratio for coherent light sources and incoherent light sources, respectively. $n_1 = 1.5$, $n_2 = 1.0$, and $\lambda = 0.6328$ μm were assumed.

The simulations to be presented require that a specified signal-to-noise ratio (SNR)

$$\text{SNR} = 10\log_{10}\left[\frac{I_s}{I_n}\right] \tag{8}$$

be maintained at the output of a PBSMBA. In our case, we have $I_s = E_0^2$ and $I_n = I_{\text{coh}}$ or I_{inc}. These are given by (6) and (7), respectively. If the optical interconnect network uses binary pulse code modulation, the signal-to-noise ratio has to be large enough to obtain the required bit error rate (BER). For a BER of 10^{-15}, the required SNR is 12 dB for using incoherent light sources and 32 dB for using coherent light sources [9]. The 20 dB difference in SNR between using coherent light and using incoherent light is due to the effect of phase-to-intensity noise conversion in avalanche photodiodes. Such difference varies with the degree of coherence and is saturated around 20 dB [9].

Because of channel cross-coupling, the interconnect distance is strongly affected by the channel separation in a dense PBSMBA. Fig. 2 shows the tradeoff between channel length and channel separation based on (6) and (7) for $n = \infty$. As indicated in Fig. 2, there is a threshold value of interconnect channel separation which decreases when increasing lateral index modulation ($n_1 - n_{3,5}$). Also, coherent and incoherent light sources lead to significant differences in interconnect distance for the same system performance. To obtain 5 cm interconnect distance, with a waveguide dimension of $a = b = 2$ μm and $n_1 - n_{3,5} = 0.006$, it may be necessary to separate the waveguides up to 12 μm (six times of channel dimension). For more favorable lateral index modulation of $n_1 - n_{3,5} = 0.015$ (the cutoff condition of a multimode channel waveguide), the required channel separation is 6 μm (as shown in Fig. 2 for coherent light). In other words, Fig. 2 indicates that the upper limit to packing density is 1250 channels/cm for a 5.0 cm long PBSMBA.

In order to find the optimum waveguide dimension, the channel separation versus waveguide dimension in a single-mode channel waveguide array was theoretically determined based on (6) and (7) for $n = \infty$, and the results plotted in Fig. 3. It indicates that larger waveguide dimension, i.e., up to the cutoff boundary of second mode (E_{12}^x), gives rise to a smaller channel separation when the lateral refractive index difference is fixed. This is because that the large waveguide dimension decreases the evanescent tail and thus increases the confinement effect. Consequently, the channel packing

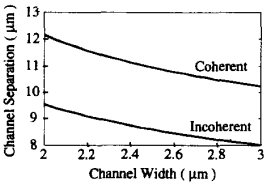

Fig. 3. Channel separation versus channel dimension based on (6) and (7). $z = 5$ cm, $a = b = 2$ μm, $n_1 = 1.5$, $n_2 = 1.0$, $n_1 - n_4 = 0.01$, and $n_1 - n_{3,5} = 0.006$ at $\lambda = 0.6328$ μm were assumed.

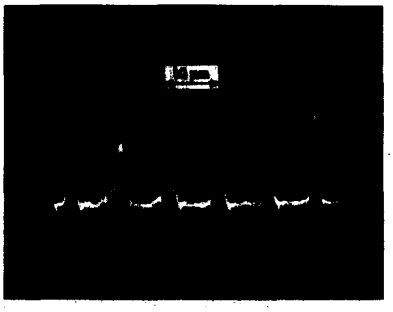

Fig. 4. Photograph of experimental result for multiple channel cross-coupling in a PBSMBA.

density can be increased or fixed while enlarging the single-mode waveguide dimension. Such a result is very useful for designing a dense single-mode channel waveguide array, where large waveguide dimension is always preferred for both coupling and fabrication. The physical parameters of a symmetric square single-mode waveguide arrray used in the calculation, can be found in Fig. 3. The signal-to-noise ratio was set at 32 dB for coherent light and 12 dB for incoherent light.

To evaluate the accuracy of the formulas developed, a 100 channel, 5 cm long single-mode waveguide array was fabricated with channel separation of $c = 8$ μm and channel width of $a = 2$ μm. Waveguide indexes $n_1 = 1.5$ and $n_1 - n_{3,5} = 0.006$ were experimentally confirmed using the IWKB method [13]. Fig. 4 is a photograph of the near field pattern of optical throughput of such a PBSMBA. In the experiment, two HeNe laser beams ($\lambda = 0.6328$ μm) with nearly uniform intensities ($I_0/I_0 = 0.85/0.95$) were coupled into the two center channel waveguides, respectively. There was no optical wave launched into the other channels at the input end, which mimics the situation of power-off with respect to the two power-on center channels in an optical binary modulation system. As indicated in Fig. 4, significant power was coupled into the side channels. It shows that the crosstalk noise due to the channel cross-coupling may seriously affect the system performance and must be considered in designing a dense PBSMBA.

Fig. 5(a) is a plot of the theoretical calculation of longitudinal intensity distribution in a PBSMBA based on (5) using the experimental parameters of Fig. 4. Input light waves with equal intensity and phase were assumed at the input end of the two center channels. Fig. 5(b) shows the transverse intensity distribution of the six center waveguides at the

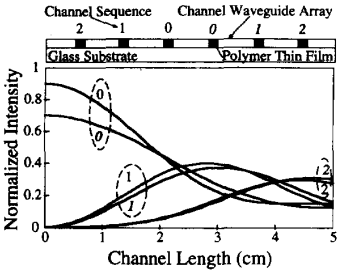

(a)

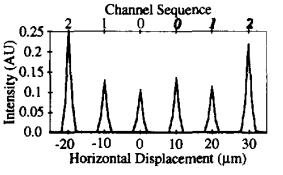

(b)

Fig. 5. (a) The intensity distribution in a PBSMBA based on (7) using the experimental parameters of Fig. 4, where $n = \infty$ was assumed. (b) The transverse intensity distribution at $z = 5$ cm.

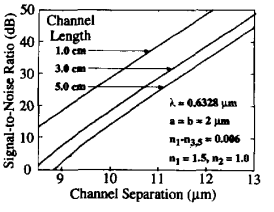

Fig. 6. Signal-to-noise ratio versus channel separation as the parameters of channel length.

propagation distance of $z = 5$ cm. The optical intensity in each channel waveguide is equivalent to Gaussian distribution with a beam waist $w = (a + \xi)$. The slight mismatch between the experimental and calculated profile for channel 2 is due to the waveguide nonuniformity.

To design an optical bus array, it would be most helpful to know the limit of channel density for which the crosstalk is low enough to be acceptable under the desired waveguide parameters. Fig. 6 shows the SNR versus channel separation as the parameter of the length of waveguide array, based on (7) and (8). In this simulation, $a = b = 2$ μm, $n_1 - n_{3,5} = 0.006$, and $\lambda = 0.6328$ μm were assumed. Based on Fig. 6, up to 12 μm channel separation is needed to keep the SNR above 32 dB at the end of the waveguide array with 5 cm length. If 40 dB SNR is required, for example, 13 μm channel separation may be needed for same waveguide parameters.

The polymer, photolime gel employed in our experiments, is a class of biopolymer consisting of thousands of 10–20 A-long amino acids. It has been classified as superpolymer because of its extraordinary chemical and physical properties and its molecular structure, which has been widely employed to fabricate holographic thin film. When the gelatin solution is subjected to temperatures below 30°C, the solution becomes a soft gel, when it is dry, it becomes a rigid glass film that shows very little absorption and optical scattering. The remarkable

fact is that the photolime gelatin has two extraordinary micro structural morphologies: 1) 2-D network—molecules are partially aligned and cross linked with inter-chain hydrogen bonds to form a helical collagen like sheet; and 2) thermoplastic → thermosetting—processible gelatin (with thermoplastic form) can be readily transformed into a highly cross-linked and insoluble polymer (with larger index of refraction) by heat of UV radiation curing. The dichromate photolime gel, doped with $((NH_4)_2Cr_2O_7)$ ammonia dichromate, can be employed to increase the optical cross-linking effect. Rib waveguide can be also fabricated through compression-molding technique during the phase transition time of the polymer based on this thermoplastic → thermosetting structural morphologies [4]. Furthermore, the (vertical) graded index characteristic of the photolime gelatin allows the formation of low loss waveguide devices on any substrate of interest [5]. The graded index property also reduces the optical scattering loss caused by the interface roughness between the polymer waveguide and its substrate.

To fabricate the photolime gel based optical channel waveguide array, the polymer thin film was first spin coated on a glass substrate. When the gelatin is first formed, it is in an aqueous solution and the molecules exist as single chains surrounded by water molecules. After standing at temperatures below 30°C, solutions of more than 1% gelatin become rigid and exhibit rubber-like mechanical properties. An optical planar waveguide region is thus formed. The formed planar waveguide was then dipped into ammonia dichromate solution for sensitization. Formation of a channel waveguide was realized by cross-linking technique through an optical mask under ultraviolet exposure. It was observed that the cross-linked area has a higher index of refraction than the unexposed area.

To introduce the desired index modulation for writing the channel waveguide on planar waveguide, based on optical cross-linking technique, the optical exposure time, t, has to be carefully controlled in the experiments, which satisfies the following equation

$$t = \frac{1}{E\beta} \ln \left[\frac{\Delta n_{\max} - \Delta n}{\Delta n_{\max}} \right] \tag{9}$$

where E is the optical intensity of the exposure beam, β is the emulsion constant related to the doping level of ammonia dichromate, the ratio of photolime gel to water, and the optical exposure wavelength. Δn is the index modulation for the exposure and $\Delta n_{\max}$ is the maximum index modulation of the material. In our experiments, $\Delta n = 0.006$, and $\Delta n_{\max} = 0.18$ were experimentally determined. The refractive index of the photolime gel, in form of planar waveguide, was measured under different UV exposure level by "VAMFO-Model 2010 Prism Coupler." With this setup, the index measurement accuracy is up to ± 0.001 with index resolution of ± 0.0005. The associated thickness measurement accuracy is $\pm(0.5\% + 50$ Å) with thickness resolution of $\pm 0.3\%$.

The channel waveguide width is defined by the optical cross-linking through a designed optical mask, where the channel waveguide pattern with designed width and separation are prewriting. In our experiments, the optical mask with channel

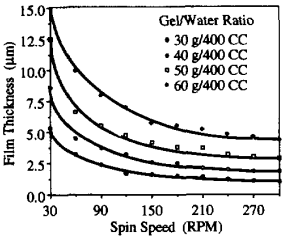

Fig. 7. Film thickness as a function of the spin speed with different gel/water ratios as a parameter.

width 2 μm and channel separation 8 μm was employed. To obtain a required waveguide thickness, the polymeric solutions with various photolime gel and water ratios were prepared and then spin-coated on glass substrates. Film thickness as a function of spin speed with photolime gel/water ratios as a parameter is shown in Fig. 7. The required thin film thickness can be obtained by choosing an appropriate spin-speed in the experiments. Stringent filtering procedure involving 1 μm filter is needed to reduce the film scattering loss associated with the material structure roughness. For the fabricated waveguide with $a = b = 2$ μm, $n_1 = 1.5$, $n_2 = 1.0$, $n_1 - n_4 \sim 0.01$, and $n_1 - n_{3,5} = 0.006$, the single-mode guiding was confirmed by the photograph of the near field pattern of the optical throughput shown in Fig. 4.

As we mentioned earlier, compression-molding technique can be also employed to mass produce large scale waveguide array using photolime gel polymer at propagation loss of 0.5 dB/cm. However, the large scale single-mode molding plungers are difficult to fabricate. For fabricating multimode channel waveguide array, the molded groove depth of the resulting rib waveguide can be controlled with 1 μm of the film thickness of 10 μm in our previous work [4]. Many important factors as the compression induced birefringence and the accuracy of small index difference produced are still under investigation and unknown at this time.

Thin film polymer-based channel waveguide arrays have the advantage of providing linear and curved optical interconnections with high packing density (1250/channel/cm) at small waveguide propagation loss of ~0.1 dB/cm and high transmission speed (60 GHz) [5], [14]. It is the only guided wave interconnection device that is technologically mass producible by compression-molded technology [4]. Also the graded index property, discovered in photolime polymer-based thin film waveguides, makes such devices particularly attractive to be fabricated on high-index and/or high loss substrates of interest, such as Si, GaAs chip and PC board [5].

In summary, a crosstalk model has been developed to study the system limitations on optical interconnects employing PBSMBA's. The upper channel packing density limit was found to be 1250 channels/cm for a 5 cm interconnect distance. This represents the first determination of packing density limit using an exact solution of the coupled-mode equations while considering channel cross-coupling among infinite number of waveguides. Computer simulations were presented together with experimental results. It was shown that there is a threshold of channel separation because of channel cross-coupling,

which results in a tradeoff between channel packing density and interconnect distance. To reduce the threshold of channel separation, high lateral index modulation is needed. Also based on the analysis, large waveguide dimension (up to the cutoff boundary of second mode (E_{12}^x)), is preferred for an optimum design in a dense PBSMBA. The analysis developed herein is applicable not only to the photolime gel PBSMBA's but also to single-mode channel waveguide bus arrays based on other materials.

REFERENCES

[1] J. P. Bristow, C. T. Sullivan, S. D. Mukherjee, Y. Liu, and A. Husain, "Progress and status of guided-wave optical interconnection technology," *Proc. SPIE*, vol. 1849, pp. 4–10, 1993.

[2] B. L. Booth, "Polymers for integrated optical waveguides," in *Polymers for Electronic and Photonic Applications*, C. P. Wong, Ed. New York: Academic, 1993, pp. 549–599.

[3] H. Takahara, S. Koike, S. Yamaguchi, and H. Tomimuro, "Optical waveguide interconnections for opto-electronic multichip modules," *Proc. SPIE*, vol. 1849, pp. 70–78, 1993.

[4] R. T. Chen, S. Tang, T. Jannson, and J. Jannson, "A 45 cm long compression molded polymer-based optical bus," *Appl. Phys. Lett.*, vol. 63, no 8, pp. 1032–1034, 1993.

[5] R. T. Chen, "Graded index linear and curved polymer channel waveguide arrays for massively parallel optical interconnects," *Appl. Phys. Lett.*, vol. 61, no. 9, pp. 2278–2280, 1992.

[6] K. Kato, K. Okamoto, H. Oazaki, Y. Ohmori, and I. Nishi, "Packaging of large-scale integrated-optic $N \times N$ star couplers," *IEEE Photon. Technol. Lett.*, vol. 4, no. 3, pp. 348–351, 1993.

[7] H. Takachashi, "10 GHz spacing optical frequency division multiplexer based on arrayed-waveguide grating," *Electron. Lett.*, vol. 28, pp. 380–382, 1992.

[8] M. Zirngibl, "Fabrication of optical splitters and wavelength routers using InP-technology," *Optics & Photon. News*, Mar., pp. 27–29, 1993.

[9] C.-S Li, C. M. Olsen, and D. G. Messershmitt, "Analysis of crosstalk penalty in dense optical chip interconnects using single-mode waveguides," *J. Lightwave Technol.*, vol. 9, no. 12, pp. 1693–1701, 1991.

[10] W. K. Burns and A. F. Milton,"Waveguide transitions and junctions," in *Guided-Wave Optoelectronics*. Berlin: Springer-Verlag, 1988, ch. 3, pp. 136–137.

[11] W. K. Burns, "Normal model analysis of waveguide devices, Part I: Theory," *J. Lightwave Technol.*, vol. 6, no. 6, pp. 1051–1057, 1988.

[12] T. K. Findakly, "Optical channel waveguides and waveguide couplers," in *Handbook of Microwave and Optical Components*. New York: Wiley, 1989, ch. 2.

[13] R. T. Chen, L. Sadovnik, T. Jannson, and J. Jannson, "Single-mode polymer waveguide modulator," *Appl. Phys. Lett.*, vol. 58, no. 1, pp. 1–3, 1991.

[14] R. T. Chen, H. Lu, D. Robinson, Z. Sun, T. Jannson, D. V. Plant, and H. R. Fetterman, "60 GHz board-to-board optical interconnection using polymer optical buses in conjunction with microprism couplers," *Appl. Phys. Lett.*, vol. 60, no. 5, pp. 536–538, 1992.

Suning Tang received the B.S. degree in electrical engineering (laser devices) from Nanjing Institute of Technology, Nanjing, China, in 1984. He received the M.Sc. in applied physics (fiber optics) from Weizmann Institute of Science, Rehovet, Israel, in 1989. He fulfilled his Ph.D. in electrical engineering (optoelectronic interconnects) from the University of Texas at Austin, Texas, in 1994. Currently, he is working as a post-doctoral fellow in the Microelectronics Research Center of the University of Texas at Austin. His current research includes planar formation of integrated intra- and inter-board optical interconnects, polymer-based guided wave devices, Si/Ge based active and passive integrated optoelectronic devices.

Dr. Tang has more than 25 publications in journals of the IEEE, OSA, and SPIE and in *Appl. Phys. Lett.* Dr. Tang is an active member of OSA and SPIE.

Ray T. Chen (M'91), for a photography and biography, see p. 1975 of the November 1994 issue of this JOURNAL.

Rob Meyer, photograph and biography not available at the time of publication.

Dave Gerold, photograph and biography not available at the time of publication.

Tomasz Jannson, photograph and biography not available at the time of publication.

Andrew Kostrzewski, photograph and biography not available at the time of publication.